Journal of Materials Chemistry A

Accepted Manuscript

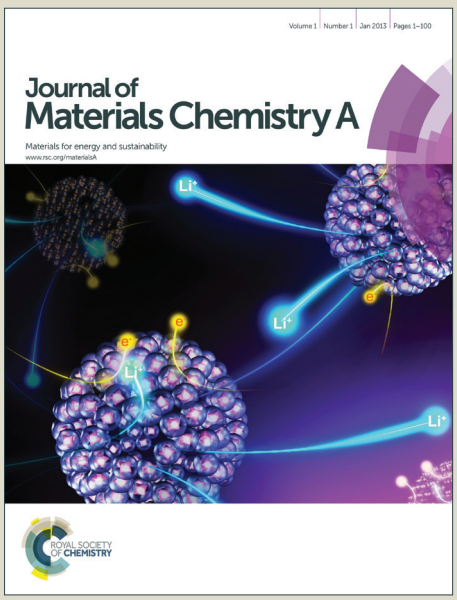

ROYAL SOCIETY OF CHEMISTRY

www.rsc.org/materialsA

Substituent Effect of Ru(II) Based Sensitizers Bearing Terpyridine Anchor and Pyridyl Azolate Ancillary for Dye Sensitized Solar Cells

Ting-Kuang Chang,[a,‡] Huiyang Li,[b,‡] Kuan-Ting Chen,[a] Yi-Chou Tsai,[a,*] Yun Chi,[a,*] Ting-Yun Hsiao,[c] and Ji-Jung Kai,[c,*]

[a] Department of Chemistry and Low Carbon Energy Research Center, National Tsing Hua University, Hsinchu 30013, Taiwan; E-mail: yictsai@mx.nthu.edu.tw, and ychi@mx.nthu.edu.tw

[b] Department of Chemistry, Hubei Key Lab on Organic and Polymeric Opto-Electronic Materials, Wuhan University, Wuhan 430072, China

[c] Department of Engineering and System Science, National Tsing Hua University, Hsinchu 30013, Taiwan; E-mail: jjkai@ess.nthu.edu.tw

[‡] These authors have equal contribution.

Abstract

In this study we explore the substituent effect of a class of Ru(II) based sensitizers bearing 4,4',4"-tricarboxy-2,2':6',2"-terpyridine anchor, functional pyridinyl azolate and a single thiocyanate ligand. Three sensitizers, i.e. PRT-tBu, ND-1 an ND-2, with t-butyl, 5-[4-[bis(4-hexyloxyphenyl)amino]phenyl]-2-thienyl and 5-[7-[4-[bis(4-hexyloxyphenyl)amino]phenyl]-4-(2,1,3-benzothiadiazolyl)]-2-thienyl substituents are designed and synthesized. Their photophysical and redox properties are probed using UV/Vis absorption and cyclic voltammetry studies. DSC cell performances (J_{SC}, V_{OC} and PCE) were also measured and analyzed in order to elucidate the structure-property relationships. It is notable that all sensitizers showed superior spectral responses in the region up to 830 nm, among which the PRT-tBu and ND-1 showed prolonged electron lifetime, suppressed electron

recombination and higher power conversion efficiency (PCE) versus the third sensitizer PRT-ND2 with benzothiadiazolyl linker at the ancillary chelate. Particularly, the optimized DSC device using PRT-tBu sensitizer gives J_{SC} of 16.29 mA cm^{-2}, V_{OC} of 787 mV and a fill factor (FF) of 0.75 corresponding to an overall PCE of 9.68 % under standard global AM 1.5 solar irradiation. Its adequate performances plus simplified synthetic procedures warrant the application in larger sized DSCs.

---

1. Introduction

Dye-sensitized solar cell (DSC) was considered an important research endeavor aimed for solving the future demands on clean, reusable and affordable electricity.[1-4] It represents a class of multidisciplinary technology that covers the wide arena of physics, chemistry, and material science and engineering.[5, 6] In terms of device designs, DSCs are composed of three functional compartments: (i) a light-harvesting dye deposited on the thin film of nanocrystalline TiO_2 and enabling injection of photoelectron,[7] (ii) an electrolyte system with suitable redox couple (most commonly I_3^-/I^-) for regeneration of the oxidized dye,[8] and (iii) an effective counter electrode (or cathode) in completing the carrier flux.[9]

In the last two decades, continuous efforts have been devoted to improve all aspects of DSC sensitizers. Thus far, Ru(II) based complexes,[10-13] zinc porphyrin,[14, 15] and even organic dyes[16-18] with push-pull charge transfer characters have shown power conversion efficiencies (PCEs) over double digits under simulated air mass 1.5 global (AM1.5G) illumination. Remarkably, the zinc porphyrin sensitizers featuring a donor-π-bridge-acceptor structure[19] and metal-free N-annulated perylene sensitizers,[20] when coupled to the cobalt(II/III) redox shuttle, both have attained the highest PCEs of up to ~13 % and 12%, respectively.

Amid various development of DSCs, the Ru(II) metal complexes are probably the

sensitizers that showed the best compromise between device efficiency and stability.[21] They are prepared using the environmental benign materials, and have achieved a reasonable PCEs of 12.0% with the employment of N749 and organic co-sensitizers; the latter is essential for offsetting the strong competitive absorption of I^-/I_3^- couple of electrolyte.[22] Importantly, as shown in Scheme 1, N749 belongs to a class of Ru(II) sensitizers which employed 4,4',4"-tricarboxy-2,2':6',2"-terpyridine (i.e. tctpy) anchor.[23] Due to the possession of three linked pyridyl units and three carboxy functional groups, this class of Ru(II) sensitizers tends to display a further red-shifted absorption onsets versus those of the 4,4'-dicarboxy-2,2'-bipyridine (i.e. dcbpy) based sensitizers, namely: N719, Z907, C101, C106 and etc. Notably, DSCs fabricated with these dcbpy based Ru(II) sensitizers are capable to exhibit high performances, i.e. PECs of ~11.1%,[24] but are still inferior to that of tctpy based N749 due to the higher onset for light absorption.

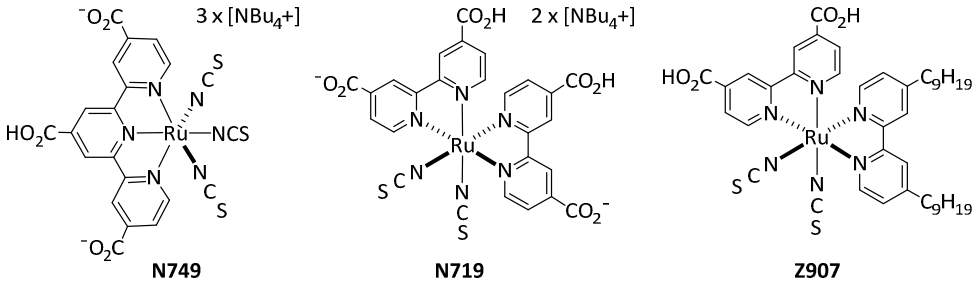

Scheme 1. Structural drawings of representative Ru(II) sensitizers N749, N719 and Z907.

Furthermore, it is known that the cell performances of DSCs depend strongly on the photosensitizing ability of sensitizers, which can be increased by introducing extended π-conjugation and/or push-pull structure to the sensitizing molecules.[25-28] In fact, similar strategies of molecular engineering have been proved successful in designing of metal-free, pure organic sensitizers.[16-18] In view of this, we then started

the preparation of three PRT based Ru(II) sensitizers, namely: PRT-tBu, PRT-ND1 and PRT-ND2, for which the differences are located at the functional groups (R) of the pyridyl azolate ancillary. The PRT-tBu sensitizer serves as the reference, for which the t-Bu substituent can reduce the dye aggregation.[29-31] Hence, their absorptions are solely deriving from chelates (i.e. both tctpy and azolate ancillary) and without the interference from various intermolecular interaction. In contrast, PRT-ND1 and PRT-ND2 are the functionalized sensitizers, on which the triarylamine has been employed for assembling of organic push-pull dyes,[32, 33] while the electron deficient 2,1,3-benzothiadiazole group[17, 34-38] is notable for its capability for inducing the charge transfer transition, respectively. Hence, we can use their differences in the absorption spectra as well as the device efficiencies to trace the substituent effects of this series of PRT sensitizers. The gained knowledge should be of useful for further improvement of sensitizers and associated DSC devices.

2. Results and Discussion

Synthesis and structural characterization. Three distinctive pyridyl azolate ancillaries, i.e. L1H, R = t-butyl, L2H, R = 5-[4-[bis(4-hexyloxyphenyl)amino]phenyl]-2-thienyl and L3H, R = 5-[7-[4-[bis(4-hexyloxyphenyl)amino]phenyl]-4-(2,1,3-benzothiadiazolyl)]-2-thienyl, were synthesized for fine-tuning the UV-Vis absorption spectral profile and, physical and photovoltaic properties. Chelate L1H was obtained using literature method,[39] while chelates L2H and L3H are synthesized using the multi-steps protocols given in the Electronic Supporting Information (ESI). Syntheses of the respective Ru(II) sensitizers were next executed using the established procedures shown in Scheme 2. They consist of sequential reaction of $RuCl_3 \cdot 3H_2O$ with 4,4',4"-triethoxycarbonyl-2,2':6',2"-terpyridine (tectpy), with 2-pyridyl azoles L1H, L2H and L3H, and finally with KSCN, giving the ethoxycarbonyl substituted Ru(II) complexes Ru1T, Ru2T and Ru3T. These products are purified by column

chromatography, while hydrolysis in mixed acetone and 2M $NaOH_{(aq)}$ afford the resulting Ru(II) sensitizers PRT-tBu, PRT-ND1 and PRT-ND2, which were collected as fine powder from the aqueous solution by adjusting to pH = 3.

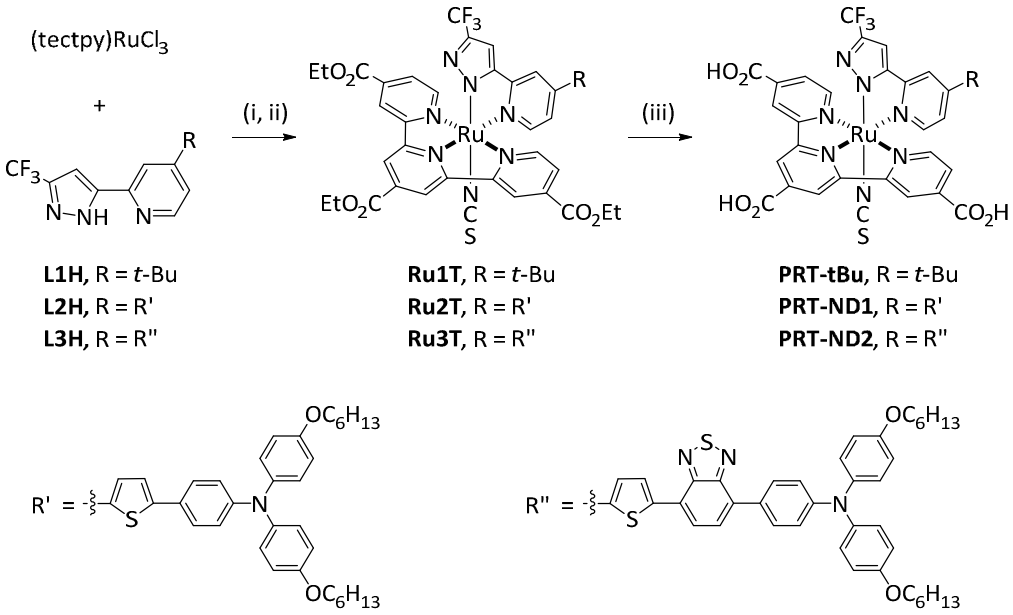

Scheme 2. (i) KOAc, toluene, reflux; (ii) DMF, KSCN, reflux; (iii) NaOH, H_2O/acetone, RT.

Photophysical behaviors. The absorption spectra of PRT-tBu, PRT-ND1 and PRT-ND2 were recorded in DMF at a concentration of 1 x 10^{-5} M, which are depicted in Figure 1, while their numeric spectral and electrochemical data are summarized in Table 1. These PRT sensitizers all display a broadened, lower intensity metal-to-ligand charge transfer (MLCT) absorption extended to ~760 nm. In addition, the PRT-tBu, ND1 and ND2 sensitizers showed another higher energy absorption band at 518, 517 and 529 nm with sequentially increased extinction coefficient (ε) of 0.85, 2.7 and 4.4 × 10^4 $M^{-1}{\cdot}cm^{-1}$, respectively. Without doubt, the higher extinction coefficient for PRT-ND1 and ND2 is due to the attached organic appendages, while the most red-shifted peak maximum and the greatest extinction coefficient of ND2 are due to

the existed, electron withdrawing benzothiadiazolyl fragment.

Upon anchored to the TiO_2 surface, all three sensitizers showed slightly broadened peak profile versus the solution spectra of each individual samples. Of particular interest is the lowest energy absorption peak, for which the onset is notably red-shifted beyond 800 nm. We attributed this to the absorption of carboxy anchor on the surface of TiO_2, for which the higher Lewis acidity of Ti^{4+} metal center is expecting to exert greater stabilization to the π*-orbital of tctpy chelate and, hence, inducing the further red-shifting of the MLCT absorption band. Notably, deposition of ethoxycarbonyl Ru(II) intermediates Ru1T, Ru2T and Ru3T on TiO_2 thin film have failed to induce any notable red-shifting of the lowest energy MLCT band, which served as an unambiguous evidence to this deduction. On the other hand, this observation is in contrast to the blue-shifting of absorption for the related Ru(II) sensitizers upon dilution or increase of pH by basification in solution.[40, 41] Proton dissociation from carboxyl anchors progressively destabilize the π*-orbital of polypyridine and, hence, increase the energy gap of MLCT transitions.

Theoretical examination. Molecular orbital calculation of the Ru(II) sensitizers was next investigated using B3LYP/6-31G* package to gain the understanding of their photophysical performances. Figure 2 presents the isodensity plots of four frontier molecular orbitals, HOMO-1 ~ LUMO+1. The HOMO-1 and HOMO of PRT-tBu are mainly populated over Ru(II) metal d_π orbitals, thiocyanate and pyrazolate fragment, while both the HOMO-1 of PRT-ND1 and ND2 have similar character versus the HOMO of PRT-tBu, but their HOMO showed significant contribution from the attached organic appendage that has the electron donating triphenylamine fragment. This observation highlights the advantage of this strategy in designing DSC sensitizers using the electron donating substituent. On the other hand, as for all sensitizers, the LUMO is solely delocalized over the unique tctpy chelate, which is consistent with the observation of the lowest energy MLCT transition located down to the longer wavelength region, i.e. 679 ~ 688 nm. Furthermore, the LUMO+1 of PRT-ND2 is

found to be significantly different from that of both PRT-tBu and ND1, by showing large contribution from the organic appendage, meaning that the electron deficient benzothiadiazolyl fragment of PRT-ND2 may serve as the sink to retard the electron injection to the TiO_2 electrode, *vide infra*.

Nevertheless, this theoretical analysis indicates that HOMO-LUMO excitation is fully capable of moving the electron density from the Ru(II) metal center, thiocyanate and pyridyl pyrazolate ancillary to the tctpy anchor. Hence, the photoinduced electron transfer from Ru(II) sensitizers to the TiO_2 electrode can occur facilely upon HOMO → LUMO excitation.

Electrochemical properties. The ground and excited-state oxidation potentials ($E^{0\prime}$ and $E^{0\prime}$*) of these PRT sensitizers are next estimated using cyclic voltammetry and the spectroscopic measurement. As shown in Table 1, all of the ground-state oxidation potentials 0.93 ~ 0.95 V (vs. NHE) are more positive than that the I^-/I_3^- redox couple (ca. 0.4 V vs. NHE), despite of various organic appendage attached at the ancillary chelate. This observation confirms the existence of adequate driving force for dye regeneration.[42-44] Moreover, the excited-state oxidation potentials of −0.85 ~ −0.87 V, which were estimated from the difference of $E^{0\prime}$ and the optical band gap (i.e. at the 5% intensity of the lowest energy absorption), and are also notably more negative than the CB potential (ca. −0.5 V vs. NHE) of nanocrystalline TiO_2, confirming the occurrence of effective electron injection.

Device performance characteristics. Sensitizers PRT-tBu, ND1 and ND2 were next employed in fabrication of DSCs. Three distinctive anodes, consisting of 5, 10 and 15 μm of 20 nm TiO_2 layer plus a 5 μm thick of scattering layer with 400 nm of TiO_2 particles, were deposited using screen-printing technique. The dye solution contained 0.3 mM of each sensitizer in mixed ethanol and *t*-butanol (v/v, 1 : 1), along with 0.6 mM of tetra-butylammonium deoxycholate [TBA][DOC] and 1 mM deoxycholic acid (DCA) as co-adsorbate. The counter electrodes were prepared from FTO glass (7 Ω/TEC7, 2.2 mm thick, Pilkington) with treatment of a PVP capped

platinum nanoclusters (PVP-Pt) via a so-called "two-step dip-coating" process, followed by post heating at 325 ^{o}C for 10 min.[45] The cells were assembled using a hot-melt Surlyn film (Meltonix 1170–25, 25 mm, Solaronix), and heated at 130 ^{o}C. Electrolyte was prepared using 0.6 M 1,2-dimethyl-3-propylimidazolium iodide (DMPII), 0.05 M lithium iodide, 0.05 M iodine, 0.1 M guanidinium thiocyanate (GuNCS), and 0.5 M *t*-butylpyridine (*t*BP) in acetonitrile. It was then injected into the cell through a pre-drilled hole at the counter electrode.

The respective device parameters are listed in Table 2, for which all reported data are averages taken from three distinctive cells, with the estimated standard deviations (esd) showed in parentheses. As expected, PRT-tBu showed the highest degree of dye loading for 5+5 μm of TiO_2 thickness due to the smallest molecular volume among all three sensitizers. However, the overall loading increases with increasing TiO_2 thickness, but the ratio is far less than the expected increase of thickness. This means that the sensitizers would be less efficient in penetrating into the void of the thicker TiO_2 layer. Eventually, these sensitizers showed dye loading of 2.37 ~ 1.63 x 10^{-7} mol cm^{-2} for DSC with 15+5 μm of TiO_2 layer.

As for the device efficiencies, PRT-ND1 showed the highest short circuit current (J_{SC}) and the highest PCE of 8.39% for cells with 5+5 μm of TiO_2 thickness. Its higher absorptivity induced by the donor appendage and π-linker are beneficial to the light harvesting. This observation is consistent with the literature report that addition of triphenylamine appendage to the class of bpy based Ru(II) sensitizers have given new sensitizers, i.e. KW1 and KW2, that display a 20% increase in PCE versus the reference compound Z907.[46] Apparently, the increased absorptivity is responsible to the improved short circuit current as well as the overall device efficiency. On the other hand, PRT-ND2, which has equally intensive peak absorptivity, produces the lowest PCE of 7.09%. This contrary must be caused by the electron accepting benzothiadiazolyl fragment, and implicated that the intense absorption cannot guarantee a higher conversion efficiency. Moreover, upon further increase of TiO_2

layer thickness to 10+5 μm and finally to 15+5 μm, due to the improved light harvesting, both of PRT-tBu and PRT-ND1 sensitizers have showed the increased PCEs of 9.68 % and 9.48%, versus the inferior PCE of 8.31% for PRT-ND2 under the identical condition. For a comparison, the commercial Z907 sensitizer exhibited a PCE of 9.06 % for cells with 15+5 μm of TiO_2 and optimized electrolyte, for which this PCE is identical to the best PCE of 9.05 % reported for DSCs with 10+5 μm of TiO_2 and same kind of electrolyte solution.[47]

The IPCEs of as-fabricated cells are shown in Figure 3(a,b,c), for which the action spectra can be separated to two sections according to the absorption wavelengths. For the DSCs with 5+5 μm of TiO_2 and with either PRT-tBu or ND1, the IPCE action spectra started at ~830 nm and rapidly increased to 55% at 750 nm and remained unchanged in the region up to 620 nm. Then, the IPCEs increased to ~70% at 550 nm, showing a better light harvesting upon moving to shorter wavelength, which reflects the higher absorptivity of sensitizers in this region. In contrast, the IPCE of PRT-ND2 only goes up to ~50% at 730 nm, increases to a maximum of 64% at 610 nm and dropped slightly to ~60% at shorter wavelength, displaying a consistently lower IPCEs versus PRT-tBu and ND1 over most of the regions.

Upon increasing the TiO_2 thickness to 15+5 μm, the IPCE of all devices imposed a notable improvement from ~55% to ~70% at the longer wavelength region. This observation could be understood in terms of the better light harvesting caused by increased dye loading. Moreover, the IPCEs of PRT-ND2 are consistently lower than those recorded for PRT-tBu and ND1 at all region, showing the deteriorating effect of the electron deficient benzothiadiazolyl unit of ancillary chelate versus the pure electron donating t-butyl and thienyl fragment.

The calculated J_{SC} was obtained by integration of IPCE response for all DSC devices. The graphical representations are showed in Figure 3(a,b,c), while numerical data are summarized in Table 2 to provide an intimate comparison with the experimental values. As can be seen, for most DSC cells, the integrated J_{SC} values are

slightly larger than the experimental data, for which the difference are attributed to the shadow mask installed to the cells. Hence, both the total incident light and J_{SC} data will be slightly reduced.

The corresponding I-V characteristics are depicted in Figure 3(d,e,f). As can be seen, PRT-tBu and ND1 sensitized solar cells gave J_{SC} = 13.04 and 14.24 mA·cm^{-2} and V_{OC} = 806 and 803 mV, respectively, for DSCs with 5+5 µm of TiO_2. Upon increased the thickness to 15+5 µm, they revealed significantly improved current density of 16.29 and 16.32 mA·cm^{-2} and slightly lowered photovoltage of 787 and 777 mV, which are consistent with better light harvesting and slightly reduced photovoltage, the latter is caused by the deteriorated coverage of sensitizer that leads to the faster electron recombination.[29] Furthermore, as for PRT-ND2, both J_{SC} and V_{OC} of the fabricated devices are systematically lowered than that of the PRT-tBu and ND1 devices. These observation is in sharp contrast to the increased efficiency observed for both organic D-A-D sensitizers[48-50] and zinc porphyrin sensitizers[51, 52] with the benzothiadiazolyl unit located near the carboxy anchor. Hence, its existence could not only increase the light harvesting, but also the electron injection into the TiO_2 acceptor. This situation is unlike to the benzothiadiazolyl unit in PRT-ND2, which is expected to induce an opposite transition dipole at the excited states and deteriorated the electron injection to the TiO_2 electrode.

Photophysical measurements of DSC devices. Charge extraction (CE) and intensity modulated photovoltage spectroscopy (IMVS) measurements were employed to study the variation of quasi-Fermi level of TiO_2 electrode[53] and differences in electron lifetimes in response to the electron recombination reaction.[54] These data are of valuable for gauging the conducting band edge (CB) of TiO_2 electrode,[55] and the interfacial energetic and dynamic origins of V_{OC} variation.[56, 57]

Figure 4a showed the extracted charge density at various recorded V_{OC} of DSC devices fabricated using sensitizers PRT-tBu, PRT-ND1, and PRT-ND2. It appears that,

at the same amount of the extracted charge density, the V_{OC} values obtained from the three dyes follows the trends of PRT-tBu > PRT-ND1 > PRT-ND2. This variation in the V_{OC} value can be explained qualitatively by a shifting in the conduction band edge (E_{CB}). Hence, the results of CE experiment indicate that the TiO_2 conduction band potential showed an upward shift in the order PRT-ND2 < PRT-ND1 < PRT-tBu, consistent with the variation of their V_{OC}.

Figure. 4b shows the plot of recombination lifetime versus V_{OC} of the studied devices, as measured from the IMVS experiments. It is notable that, at any given V_{OC}, the PRT-tBu sensitizer showed the longest lifetime versus all other sensitizers. This result indicated that the charge recombination was the slowest for PRT-tBu, followed by PRT-ND1, while the PRT-ND2 had the fastest recombination. Apparently, the electron deficient 2,1,3-benzothiadiazole unit, although it is not located in the close vicinity of TiO_2 surface as showed in the recently reported zinc prophyrin sensitizers,[51, 52] it still showed substantial increase in charge recombination, causing shorter electron lifetime and lower V_{OC} than that of other sensitizers. Overall, these combined results indicated that different donor in this class of Ru(II) sensitizers would have substantially influence on both the CB edge of TiO_2 as well as the charge recombination at the same time.

Stability measurement and fabrication of large sized modules. For evaluation of the long-term stability of the as-fabricated DSCs, the electrolyte was switched to a mixture of 1 M 1,3-dimethylimidazolium iodide (DMII), 0.1 M sodium iodide, 0.15 M iodine, 0.1 M guanidinium thiocyanate (GuNCS), and 0.5 M N-butyl benzimidazole (NBB) dissolved in butyronitrile.[58] The performance evolutions of all three DSC cells are summarized in Figure 5. Over the entire period of 1000 h at 60 °C under accelerated visible-light soaking, the photovoltaic parameters J_{SC}, V_{OC}, *FF* of PRT-tBu and ND1 based cells showed a consistently higher values versus those of the PRT-ND2, despite there are random fluctuation of performance parameters. Particular interested is the data recorded for PRT-tBu, for which the final PCE of

9.01 %, is almost identical to its maxima PCE of 9.27 % recorded only after 300 h. This excellent stability indicates the advantage of PRT-tBu for fabrication of both thermally stable and larger sized sloar cell modules.

As showed in Figure 6, the larger sized DSC cell consists of four parallel TiO_2 strips, each with a 15+5 μm of the absorbing (20 nm) plus light scattering (400 nm) of TiO_2 layer and with an active area of 4 x 0.98 x 5.7 cm^2 (e.g. 22.3 cm^2). The cell was fabricated using routine assembling protocol established for the aforementioned small sized DSCs, except that, a grid of silver wires was printed on the TiO_2 photoanode and the counter electrode using commercial silver paste for better collecting the photocurrent. The grid on counter electrode is next covered with glass cement for protection against the corrosion induced by electrolyte and, next, the cell was carefully assembled using Surlyn and for ensuring good insulation around the silver grid. This type of DSC cell with PRT-tBu sensitizer shows a J_{SC} of 16.25 $mA{\cdot}cm^{-2}$, a V_{OC} of 690 mV, and FF of 0.57 under the standard AM 1.5 G solar irradiation and without shadow mask. It is notable that both the observed J_{SC} and V_{OC} are similar to those of the smaller sized DSC cells, while the large decrease in FF is due to the inefficient collection of photocurrent at the electrodes and the increased diffusion resistivity of the redox electrolyte. The active-area PCE of 6.32 % can be calculated using this set of data. However, the calculated PCE is dropped to 5.96 %, upon using a shadow mask with aperture area of 4.8 x 5.92 (or 28.4) cm^2, for which the non-active areas of ~21 % (i.e. 28.4 – 22.3 = 6.1 cm^2) is attributed to the area required for applying Surlyn that glue together the front and back panels. As a reference, similar large-sized DSC cell based on commercial Z907 sensitizer was also fabricated using identical architecture and the corresponding optimized electrolyte system. The obtained device characteristics, i.e. J_{SC} of 13.28 $mA{\cdot}cm^{-2}$, V_{OC} of 740 mV, FF of 0.50 and overall PCE of 4.91 %, are significant lower, which unambiguously assure the superiority of our current design of sensitizer.

3. Conclusion

Three 4,4',4"-triethoxycarbonyl-2,2':6',2"-terpyridine based Ru(II) sensitizers, i.e. PRT-tBu, ND-1 an ND-2, with t-butyl, 5-[4-[bis(4-hexyloxyphenyl)amino]phenyl]-2-thienyl and 5-[7-[4-[bis(4-hexyloxyphenyl)amino]phenyl]-4-(2,1,3-benzothiadiazolyl)]-2-thienyl substituents on the pyridyl azolate ancillary are synthesized and tested for fabrication of DSC devices. Disregarding to the lower absorptivity of PRT-tBu versus the functionalized PRT-ND1 and ND2, the sensitizers PRT-tBu and ND1 displayed comparable PCEs (9.68 and 9.48 %), and both were superior to the third sensitizer PRT-ND2 (PCE = 8.31 %) which possessed the electron withdrawing benzothiadiazolyl bridge for inducing the occurrence of charge transfer absorption. However, as showed by the CE and IMVS measurements, this benzothiadiazolyl group has unfortunately induced a downward shifting of CB edge of TiO_2 and a relatively increased electron recombination, giving the systematically inferior device efficiencies. Moreover, due to an ample supply of its ancillary chelate, PRT-tBu has been obtained in larger quantity to allow the fabrication of larger-sized DSC devices and modules possible. The enlarged device has an active-area of 22.3 cm^2 and displays performances: J_{SC} = 13.01 $mA{\cdot}cm^{-2}$, V_{OC} = 680 mV, FF = 0.57 and active-area PCE = 5.96 %. Hence, the gained experiences should be of valuable to the future design of larger sized commercial DSCs and modules.

4. Experimental section

General Procedures. All reactions were performed under nitrogen and were monitored by TLC with pre-coated silica gel plates (Merck, 0.20 mm with UV254 indicator). Column chromatography was carried out using silica gel obtained from Merck (230 - 400 mesh). Mass spectra were obtained on a JEOL SX-102A instrument. ^1H and ^{19}F NMR spectra were recorded on a Varian Mercury-400 instrument. Elemental analysis was carried out with a Heraeus CHN-O Rapid Elementary Analyzer.

Photophysical data were obtained using an Edinburgh Fluorescence spectrometer FLS928P.

Synthesis of ethoxycarbonyl derivatives Ru1T – Ru3T. Synthetic procedures are similar to those employed for the other PRT series of sensitizers.[59, 60] A solution of (tectpy)$RuCl_3$ (723 mg, 1.1 mmol), **L1H** (269 mg, 1.0 mmol) and KOAc (196 mg, 2.0 mmol) in toluene was heated under reflux for 4h. After cooling to RT, the solvent was removed and the residue was dissolved in CH_2Cl_2, washed with water, dried over Na_2SO_4, and concentrated to dryness. The crude product was purified using column chromatography to give **Ru1Cl** as a black solid (570 mg, 67%). The other Ru(II) complexes **Ru2Cl** (400 mg, 73%) and **Ru3Cl** (103 mg, 60%) were synthesized using chelates **L2H** and **L3H** under similar condition.

Next, a DMF solution of **Ru1Cl** (415 mg, 0.46 mmol) and KSCN (236 mg, 2.43 mg) was heated under reflux overnight. After cooling to RT, the solvent was removed and the residue was dissolved in CH_2Cl_2. This solution was extracted with water, dried over anhydrous Na_2SO_4, and evaporated to dryness. The obtained product was purified using column chromatography to give compound **Ru1T** as a black solid (300 mg, 70%). Complexes **Ru2T** (125 mg, 57%) and **Ru3T** (102 mg, 60%) were synthesized in a similar manner.

Spectral data of **Ru1T**: ^{1}H NMR (400 MHz, $CDCl_3$, 298 K): δ 9.41 (d, *J* = 6.0 Hz, 1H), 8.82 (s, 2H), 8.71 (s, 2H), 7.87 (d, *J* = 5.6 Hz, 2H), 7.80 - 7.76 (m, 3H), 7.59 (d, *J* = 4.8 Hz, 1H), 6.73 (s, 1H), 4.66 - 4.61 (m, 2H), 4.50 - 4.44 (m, 4H), 1.59 (t, *J* = 7.2 Hz, 3H), 1.54 (s, 9H), 1.43 (t, *J* = 7.0 Hz, 6H). ^{19}F NMR (376 MHz, $CDCl_3$, 298K): δ -60.44 (s, 3F).

Spectral data of **Ru2T**: ^{1}H NMR (400 MHz, $CDCl_3$, 298 K): δ 9.43 (d, *J* = 6.0 Hz, 1H), 8.82 (s, 2H), 8.70 (s, 2H), 7.95 (s, br, 3H), 7.77 (dd, *J* = 5.6 Hz, *J* = 1.6 Hz, 2H), 7.72 (d, *J* = 5.2 Hz, 1H), 7.69 (d, *J* = 4.0 Hz, 1H), 7.50 (d, *J* = 8.4 Hz, 2H), 7.31 (d, *J* = 4.0 Hz, 1H), 7.10 (d, *J* = 5.2 Hz, 4H), 6.96 (d, *J* = 8.8 Hz, 2H), 6.86 (d, *J* = 9.2 Hz, 4H), 6.80 (s, 1H), 4.67 - 4.61 (m, 2H), 4.50 - 4.45 (m, 4H), 3.96 (t, *J* = 6.4 Hz, 4H), 1.83 - 1.76 (m, 4H), 1.60 (t, *J* = 7.2 Hz, 3H), 1.51 - 1.42 (m, 10H), 1.38 - 1.33 (m, 8H), 0.92 (t, *J* = 7.0 Hz,

6H). ^{19}F NMR (376 MHz, $CDCl_3$, 298K): δ -60.42 (s, 3F).

Spectral data of **Ru3T**: ^{1}H NMR (400 MHz, $CDCl_3$, 298 K): δ 9.48 (d, *J* = 6.0 Hz, 1H), 8.82 (s, 2H), 8.70 (s, 2H), 8.21 (d, *J* = 3.6 Hz, 1H), 8.05 - 8.03 (m, 2H), 7.94 (s, br, 2H), 7.86 - 7.79 (m, 4H), 7.77 - 7.72 (m, 3H), 7.13 (d, *J* = 8.4 Hz, 4H), 7.05 (d, *J* = 8.4 Hz, 2H), 6.86 (d, *J* = 8.4 Hz, 4H), 4.65 - 4.60 (m, 2H), 4.48 - 4.43 (m, 4H), 3.94 (t, *J* = 6.4 Hz, 4H), 1.82 - 1.74 (m, 4H), 1.58 (t, *J* = 7.2 Hz, 3H), 1.50 - 1.40 (m, 10H), 1.36 - 1.32 (m, 8H), 0.90 (t, *J* = 6.6 Hz, 6H). ^{19}F NMR (376 MHz, $CDCl_3$, 298K): δ -60.40 (s, 3F).

Synthesis of PRT-tBu, PRT-ND1 and PRT-ND2. To an acetone (150 mL) solution of **Ru1T** (193 mg, 0.22 mmol) was added an aqueous solution of NaOH (2M, 10 mL). The mixture was stirred at RT overnight. It was then concentrated to approx. 30 mL and pH was adjusted to 3 by addition of 2M HCl solution. The precipitation was collected, washed with water, acetone and ether in sequence to obtain PRT-tBu as a brown solid (162 mg, 93%). Sensitizers PRT-ND1 (72 mg, 66%) and PRT-ND2 (102 mg, 69%) were synthesized in a similar manner.

Spectral data of PRT-tBu: MS (FAB, ^{102}Ru): *m/z* 793 $[M]^+$. ^{1}H NMR (400 MHz, d_6-DMSO, 298 K): δ 13.93 (s, br, 3H), 9.21 (s, 2H), 9.19 (d, *J* = 6.0 Hz, 1H), 9.07 (s, 2H), 8.18 (d, *J* = 2.0 Hz, 1H), 7.89 (d, *J* = 6.0 Hz, 2H), 7.87 - 7.84 (m, 3H), 7.16 (s, 1H), 1.48 (s, 9H). ^{19}F NMR (376 MHz, d_6-DMSO, 298 K): δ -58.48. Anal. calcd. for $C_{32}H_{24}F_3N_7O_6RuS{\cdot}3H_2O$: C, 45.39; N, 11.58; H, 3.57. Found: C, 45.60; N, 11.48; H, 3.70.

Spectral data of PRT-ND1: MS (FAB, ^{102}Ru): *m/z* 1263 $[M + H]^+$. ^{1}H NMR (400 MHz, d_6-DMSO, 298 K): δ 9.21 - 9.19 (m, 3H), 9.07 (s, 2H), 8.46 (s, 1H), 8.08 (d, *J* = 4.0 Hz, 1H), 8.05 - 8.01 (m, 3H), 7.82 (dd, *J* = 5.6 Hz, *J* = 1.6 Hz, 2H), 7.58 - 7.55 (m, 3H), 7.21 (s, 1H), 7.04 (d, *J* = 8.8 Hz, 4H), 6.91 (d, *J* = 8.8 Hz, 4H), 6.79 (d, *J* = 8.8 Hz, 2H), 3.92 (t, *J* = 6.4 Hz, 4H), 1.71 - 1.64 (m, 4H), 1.42 - 1.35 (m, 4H), 1.30 - 1.27 (m, 8H), 0.85 (t, *J* = 7.0 Hz, 6H). ^{19}F NMR (376 MHz, d_6-DMSO, 298 K): δ -58.48. Anal. calcd. for $C_{62}H_{55}F_3N_8O_8RuS_2{\cdot}3H_2O$: C, 56.57; N, 8.51; H, 4.67. Found: C, 56.89; N, 8.56; H, 4.96.

Spectral data of PRT-ND2: MS (FAB, ^{102}Ru): *m/z* 1396 $[M]^+$. ^{1}H NMR (400 MHz,

d_6-DMSO, 298 K): δ 9.27 (d, *J* = 6.0 Hz, 1H), 9.19 (s, 2H), 9.05 (s, 2H), 8.56 (s, 1H), 8.31 (d, *J* = 4.0 Hz, 1H), 8.25 (d, *J* = 7.6 Hz, 1H), 8.22 (d, *J* = 3.6 Hz, 1H), 8.11 (d, *J* = 5.6 Hz, 1H), 8.06 (d, *J* = 6.0 Hz, 2H), 7.90 (d, *J* = 8.8 Hz, 2H), 7.87 (d, *J* = 7.6 Hz, 1H), 7.81 (d, *J* = 6.0 Hz, 2H), 7.27 (s, 1H), 7.06 (d, *J* = 8.8 Hz, 4H), 6.91 (d, *J* = 9.2 Hz, 4H), 6.86 (d, *J* = 8.8 Hz, 2H), 3.91 (t, *J* = 6.6 Hz, 4H), 1.71 - 1.64 (m, 4H), 1.42 - 1.35 (m, 4H), 1.30 - 1.26 (m, 8H), 0.85 (t, *J* = 7.0 Hz, 6H). ^{19}F NMR (376 MHz, d_6-DMSO, 298 K): δ -58.48. Anal. calcd. for $C_{68}H_{57}F_3N_{10}O_8RuS_3 \cdot 3H_2O$: C, 56.30; N, 9.66; H, 4.38. Found: C, 56.76; N, 9.69; H, 4.69.

Device fabrication. The pre-cleaned FTO glasses (4 mm thickness, Nippon Sheet Glass Co., Japan) were immersed in a 40 mM aqueous $TiCl_4$ solution at 70 ^oC for 30 min, followed by washing with water and ethanol. They were then deposited with 5, 10, 15 μm of 20 nm TiO_2 particles, followed by a 5 μm scattering layer containing 400 nm TiO_2 particles (PST-400, JGC Catalysts and Chemicals, Japan). The TiO_2 electrodes were heated in air at 325 ^oC for 30 min, followed by heating at 375 ^oC for 5 min, 450 ^oC for 15 min, and 500 ^oC for 30 min. They were next treated with 40 mM aqueous solution of $TiCl_4$ for 30 min at 70 ^oC, followed by heating at 500 ^oC for 30 min. Subsequently, these TiO_2 films were immersed in a dye solution for 18 h at 25 ^oC, which were prepared using absolute ethanol and *t*-butanol (v/v, 1 : 1).

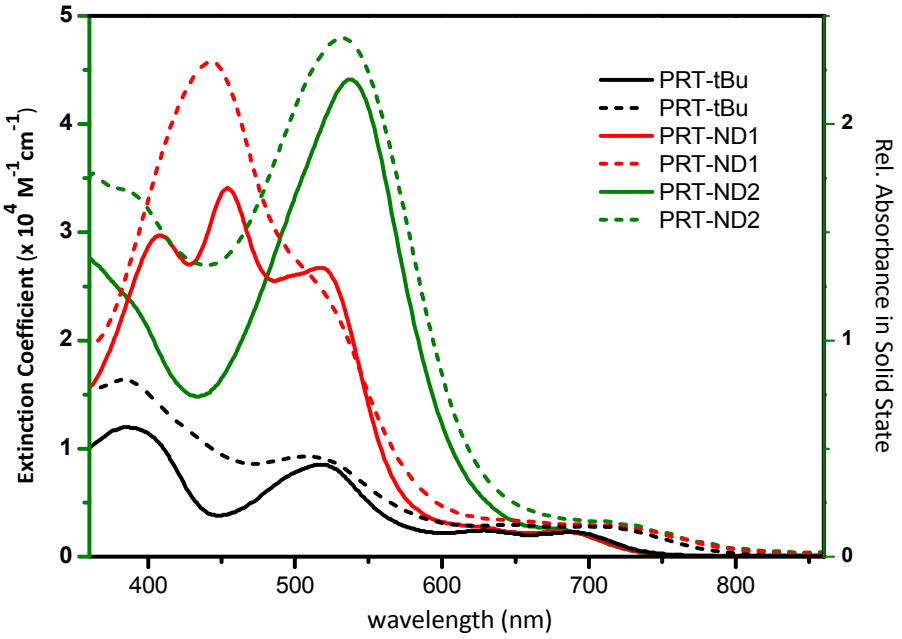

Figure 1. UV-Vis absorption spectra of PRT-tBu, PRT-ND1 and PRT-ND2 in DMF (solid line, left axis) and those deposited on 6 µm of 20 nm, TiO_2 layer (dash line, right axis in arbitrary unit).

	HOMO-1	HOMO	LUMO	LUMO+1
a	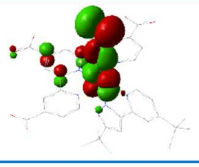	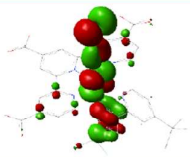	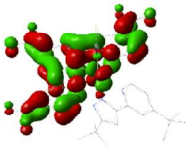	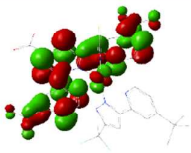
	-0.2062 eV	-0.1979 eV	-0.1076 eV	-0.0934 eV
b	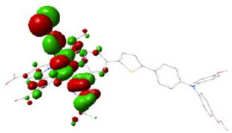	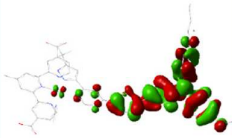	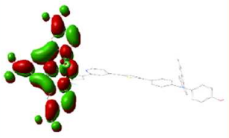	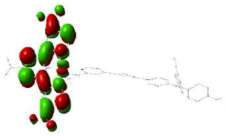
	-0.1981 eV	-0.1773 eV	-0.1076 eV	-0.0934 eV
c	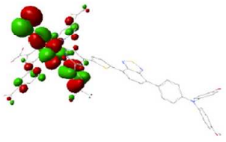	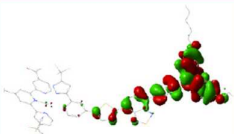	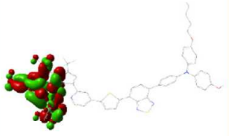	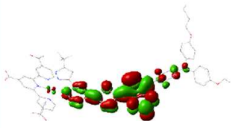
	-0.1985 eV	-0.1777 eV	-0.1078 eV	-0.0989 eV

Figure 2. Isodensity plots of four frontier molecular orbitals for (a) PRT-tBu, (b) PRT-ND1 and (c) PRT-ND2.

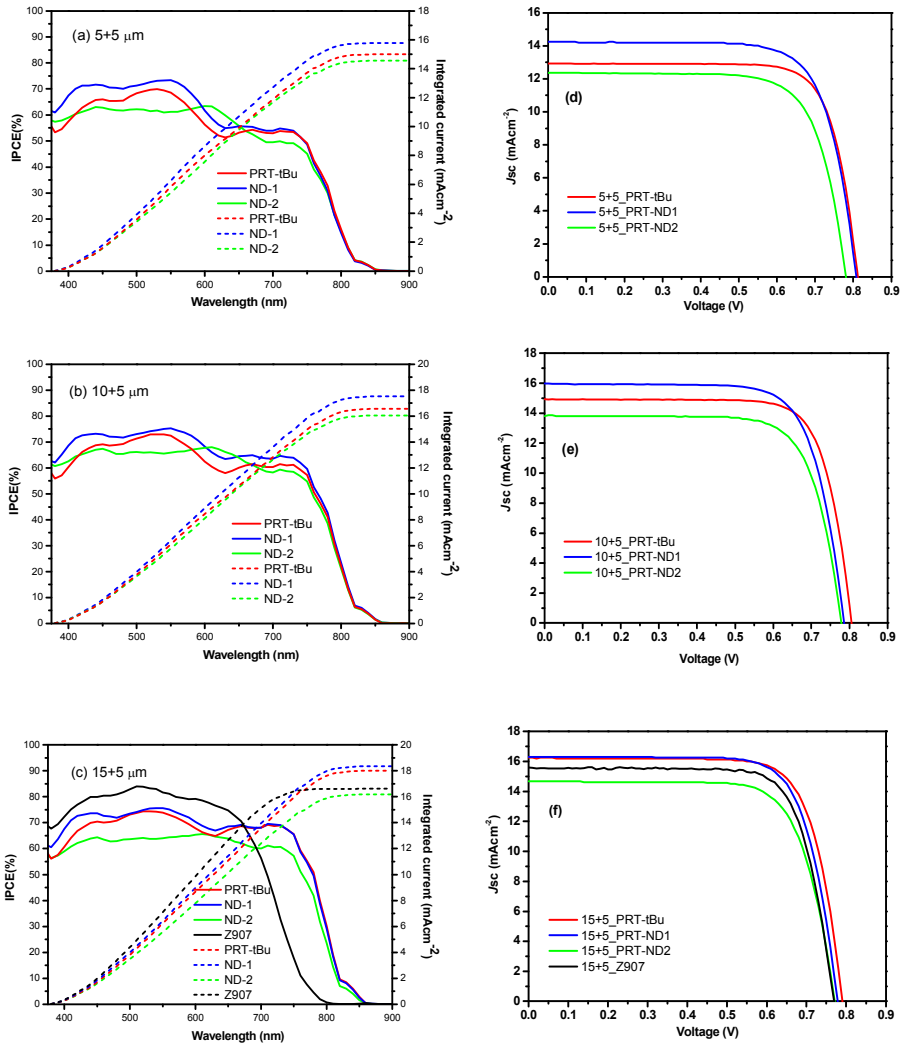

Figure 3. Incident photon-to-electron conversion efficiency (IPCE) action spectra, integrated current density, I-V characteristics of DSCs with different TiO_2 thickness of 5+5, 10+5 and 15+5 μm and with sensitizers PRT-tBu, ND1 and ND2.

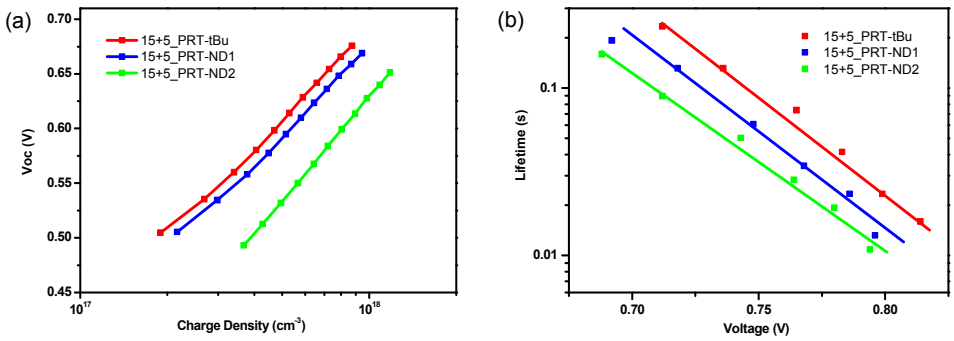

Figure 4. (a) TiO_2 electron density versus voltage deduced from CE measurements and (b) electron lifetime versus TiO_2 electron density deduced from IMVS measurements for DSC devices containing PRT-tBu and ND1 and ND2. The cell voltage is controlled via tuning the illumination from a halogen lamp.

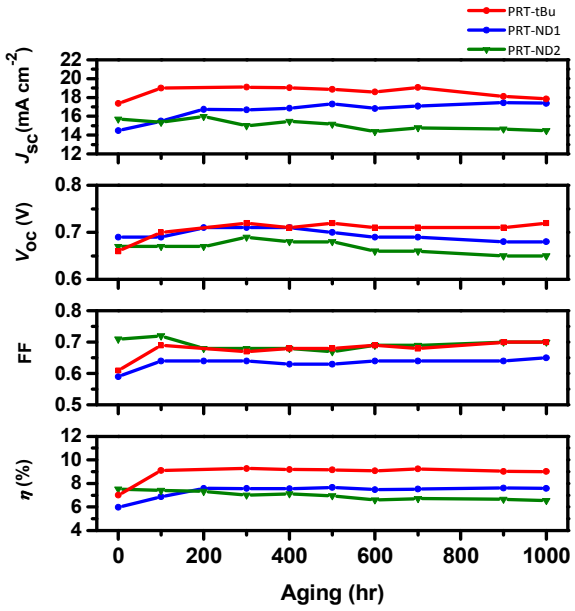

Figure 5. Device performances of all studied DSCs under one-sun light soaking at 60 °C for 1000 h. Electrolyte is composed of 1 M DMII, 0.15 M I_2, 0.1 M NaI, 0.1 M GuNCS, and 0.5 M NBB in butyronitrile.

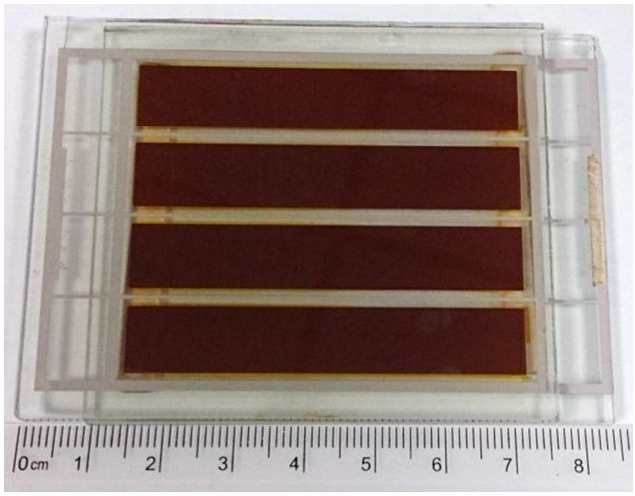

Figure 6. Photograph of a larger sized DSC module.

Table 1. Absorbance and electrochemical properties of the studied Ru(II) sensitizers

Sensitizer	λ_{max} (nm; $\varepsilon \times 10^3$ M^{-1} cm^{-1}) [a]	$E_{0\text{-}0}$ [b](eV)	E_{ox} [c](V) NHE	E_{red} [d](V) NHE
PRT-tBu	385 (12); 518 (8.5); 688 (2.3)	1.81	0.95	-0.86
PRT-ND1	408 (29.7); 454 (34.1); 517 (26.7); 679 (2.3)	1.78	0.93	-0.85
PRT-ND2	539 (44.1) ; 680 (2.3)	1.81	0.94	-0.87

[a] Absorption spectra of sensitizers measured in DMF with the concentration of 1 x 10^{-5} mol L^{-1}. [b] The bandgap, E_{0-0} was derived the intersection of the absorption and tangent of the emission peak in DMF. [c] E_{ox} were measured in DMF with 0.1 M $(^nBu)_4NPF_6$ as electrolyte. It was calibrated with FcH/FcH^+ as internal reference and converted to NHE by addition of 0.63 V. [d] E_{red} was calculated according to equation $E_{ox} - E_{0\text{-}0}$.

Table 2. The performances for DSCs measured under AM1.5G one sun irradiation.

sensitizer	J_{SC} [mA cm^{-2}]	J_{SC} calc. from IPCE	V_{OC} [mV]	FF	PCE [%]	loading [x 10^{-7} mol cm^{-2}]
PRT-tBu[a]	13.04(32)	15.00	806(6)	0.77(1)	8.09(13)	1.11
PRT-tBu[b]	14.89(22)	16.58	800(10)	0.76(1)	9.11(10)	1.46
PRT-tBu[c]	16.29(11)	18.01	787(7)	0.75(1)	9.68(14)	2.37
PRT-ND1[a]	14.24(19)	15.78	803(7)	0.74(1)	8.39(16)	0.72
PRT-ND1[b]	15.95(15)	17.54	787(7)	0.73(1)	9.23(5)	1.01
PRT-ND1[c]	16.32(08)	18.35	777(7)	0.75(1)	9.48(4)	1.76
PRT-ND2[a]	12.57(86)	14.53	777(7)	0.73(2)	7.09(19)	0.75
PRT-ND2[b]	14.05(28)	16.06	777(7)	0.73(1)	7.94(15)	0.95
PRT-ND2[c]	15.05(15)	16.17	767(7)	0.72(4)	8.31(9)	1.63
Z907[c,d]	15.60(31)	16.62	770(6)	0.75(1)	9.06(10)	

The devices were fabricated using [a] 5+5, [b] 10+5 and [c] 15+5 μm of TiO_2 layers with an area of 5 x 5 mm^2. The first and second digit stand for the thickness of small (20 nm) and large (400 nm) TiO_2 particles. Device performances were measured using a black metal mask with an aperture area of 4 × 4 mm^2. The loading is calculated from the absorption intensity of desorbed dye solution versus a reference solution with 0.01 mM of dye and 0.1 M of [TBA]OH in a 1:1 (v:v) mixture of MeOH and water. [d] Electrolyte of Z907 device is composed of 1 M DMII, 0.03 M I_2, 0.05 M LiI, 0.1 M GuNCS, and 0.5 M TBP in AN/VN (85/15).

1. A. Hagfeldt, G. Boschloo, L. Sun, L. Kloo and H. Pettersson, *Chem. Rev.*, 2010, **110**, 6595.
2. S. Zhang, X. Yang, Y. Numata and L. Han, *Energy Environ. Sci.*, 2013, **6**, 1443.
3. K. G. Reddy, T. G. Deepak, G. S. Anjusree, S. Thomas, S. Vadukumpully, K. R. V. Subramanian, S. V. Nair and A. S. Nair, *Phys. Chem. Chem. Phys.*, 2014, **16**, 6838.
4. N. Sharifi, F. Tajabadi and N. Taghavinia, *ChemPhysChem*, 2014, **15**, 3902.
5. A. Fakharuddin, R. Jose, T. M. Brown, F. Fabregat-Santiago and J. Bisquert, *Energy Environ. Sci*, 2014, **7**, 3952.
6. M. Ye, X. Wen, M. Wang, J. Iocozzia, N. Zhang, C. Lin and Z. Lin, *Mater. Today*, 2015, **18**, 155.
7. Y. Bai, I. Mora-Seró, F. De Angelis, J. Bisquert and P. Wang, *Chem. Rev.*, 2014, **114**, 10095.
8. J. Wu, Z. Lan, J. Lin, M. Huang, Y. Huang, L. Fan and G. Luo, *Chem. Rev.*, 2015, **115**, 2136.
9. S. Thomas, T. G. Deepak, G. S. Anjusree, T. A. Arun, S. V. Nair and A. S. Nair, *J. Mater. Chem. A*, 2014, **2**, 4474.
10. G. C. Vougioukalakis, A. I. Philippopoulos, T. Stergiopoulos and P. Falaras, *Coord. Chem. Rev.*, 2011, **255**, 2602.
11. P. G. Bomben, K. C. D. Robson, B. D. Koivisto and C. P. Berlinguette, *Coord. Chem. Rev.*, 2012, **256**, 1438.
12. Y. Chi, B. Tong and P.-T. Chou, *Coord. Chem. Rev.*, 2014, **281**, 1.
13. Y. Chi, K.-L. Wu and T.-C. Wei, *Chem. Asian J.*, 2015, **10**, 1098.
14. L.-L. Li and E. W.-G. Diau, *Chem. Soc. Rev.*, 2013, **42**, 291.
15. T. Higashino and H. Imahori, *Dalton Trans.*, 2015, **44**, 448.
16. S. Ahmad, E. Guillen, L. Kavan, M. Gratzel and M. K. Nazeeruddin, *Energy Environ. Sci.*, 2013, **6**, 3439.
17. Y. Wu and W. Zhu, *Chem. Soc. Rev.*, 2013, **42**, 2039.
18. C.-P. Lee, R. Y.-Y. Lin, L.-Y. Lin, C.-T. Li, T.-C. Chu, S.-S. Sun, J. T. Lin and K.-C. Ho, *RSC Adv.*, 2015, **5**, 23810.
19. S. Mathew, A. Yella, P. Gao, R. Humphry-Baker, F. E. CurchodBasile, N. Ashari-Astani, I. Tavernelli, U. Rothlisberger, M. K. Nazeeruddin and M. Grätzel, *Nat. Chem.*, 2014, **6**, 242.
20. Z. Yao, M. Zhang, R. Li, L. Yang, Y. Qiao and P. Wang, *Angew. Chem. Int. Ed.*, 2015, **54**, 5994.
21. J.-F. Yin, M. Velayudham, D. Bhattacharya, H.-C. Lin and K.-L. Lu, *Coord. Chem. Rev.*, 2012, **256**, 3008.
22. L. Han, A. Islam, H. Chen, C. Malapaka, B. Chiranjeevi, S. Zhang, X. Yang and M. Yanagida, *Energy Environ. Sci.*, 2012, **5**, 6057.
23. M. K. Nazeeruddin, P. Péchy, T. Renouard, S. M. Zakeeruddin, R. Humphry-Baker, P. Comte, P. Liska, L. Cevey, E. Costa, V. Shklover, L. Spiccia, G. B. Deacon, C. A. Bignozzi and M. Grätzel, *J. Am. Chem. Soc.*, 2001, **123**, 1613.
24. Y. Numata, S. P. Singh, A. Islam, M. Iwamura, A. Imai, K. Nozaki and L. Han, *Adv. Funct. Mater.*, 2013, **23**, 1817.
25. W. Zeng, Y. Cao, Y. Bai, Y. Wang, Y. Shi, M. Zhang, F. Wang, C. Pan and P. Wang, *Chem. Mater.*, 2010, **22**, 1915.
26. Y. Wang, L. Yang, M. Xu, M. Zhang, Y. Cai, R. Li and P. Wang, *J. Phys. Chem. C*, 2014, **118**, 16441.
27. K.-L. Wu, Y. Hu, C.-T. Chao, Y.-W. Yang, T. Y. Hsiao, N. Robertson and Y. Chi, *J. Mater. Chem. A*, 2014, **2**, 19556.
28. C.-G. Wu, C. Lee and S.-J. Wu, *J. Mater. Chem. A*, 2014, **2**, 17551.
29. K.-L. Wu, W.-P. Ku, J. N. Clifford, E. Palomares, S.-T. Ho, Y. Chi, S.-H. Liu, P.-T. Chou, M. K. Nazeeruddin and M. Grätzel, *Energy Environ. Sci.*, 2013, **6**, 859.
30. C.-C. Chou, F.-C. Hu, H.-H. Yeh, H.-P. Wu, Y. Chi, J. N. Clifford, E. Palomares, S.-H. Liu, P.-T. Chou and G.-H. Lee, *Angew. Chem. Int. Ed.*, 2014, **53**, 178.
31. H.-Y. Ku, B. Tong, Y. Chi, H.-C. Kao, C.-C. Yeh, C.-H. Chang and G.-H. Lee, *Dalton*

Trans., 2015, **44**, 8552.
32. H. Hayashi, A. S. Touchy, Y. Kinjo, K. Kurotobi, Y. Toude, S. Ito, H. Saarenpaeae, N. V. Tkachenko, H. Lemmetyinen and H. Imahori, *ChemSusChem*, 2013, **6**, 508.
33. A. Kokil, J. M. Chudomel, P. J. Homnick, P. M. Lahti and J. Kumar, *RSC Adv.*, 2013, **3**, 15626.
34. W. Zhu, Y. Wu, S. Wang, W. Li, X. Li, J. Chen, Z.-s. Wang and H. Tian, *Adv. Funct. Mater.*, 2011, **21**, 756.
35. S. Haid, M. Marszalek, A. Mishra, M. Wielopolski, J. Teuscher, J.-E. Moser, R. Humphry-Baker, S. M. Zakeeruddin, M. Grätzel and P. Baeuerle, *Adv. Funct. Mater.*, 2012, **22**, 1291.
36. R. Stalder, D. Xie, A. Islam, L. Han, J. R. Reynolds and K. S. Schanze, *ACS Appl. Mater. Int.*, 2014, **6**, 8715.
37. X. Kang, J. Zhang, D. O'Neil, A. J. Rojas, W. Chen, P. Szymanski, S. R. Marder and M. A. El-Sayed, *Chem. Mater.*, 2014, **26**, 4486.
38. M. Katono, M. Wielopolski, M. Marszalek, T. Bessho, J.-E. Moser, R. Humphry-Baker, S. M. Zakeeruddin and M. Grätzel, *J. Phys. Chem. C*, 2014, **118**, 16486.
39. L.-M. Huang, G.-M. Tu, Y. Chi, W.-Y. Hung, Y.-C. Song, M.-R. Tseng, P.-T. Chou, G.-H. Lee, K.-T. Wong, S.-H. Cheng and W.-S. Tsai, *J. Mater. Chem. C*, 2013, **1**, 7582.
40. S.-W. Wang, K.-L. Wu, E. Ghadiri, M. G. Lobello, S.-T. Ho, Y. Chi, J.-E. Moser, F. De Angelis, M. Grätzel and M. K. Nazeeruddin, *Chem. Sci.*, 2013, **4**, 2423.
41. C.-C. Chou, F.-C. Hu, K.-L. Wu, T. Duan, Y. Chi, S.-H. Liu, G.-H. Lee and P.-T. Chou, *Inorg. Chem.*, 2014, **53**, 8593.
42. M. Planells, L. Pelleja, J. N. Clifford, M. Pastore, F. De Angelis, N. Lopez, S. R. Marder and E. Palomares, *Energy Environ. Sci.*, 2011, **4**, 1820.
43. A. Listorti, B. O'Regan and J. R. Durrant, *Chem. Mater.*, 2011, **23**, 3381.
44. A. Y. Anderson, P. R. F. Barnes, J. R. Durrant and B. C. O'Regan, *J. Phys. Chem. C*, 2011, **115**, 2439.
45. T.-C. Wei, C.-C. Wan, Y.-Y. Wang, C.-M. Chen and H.-S. Shiu, *J. Phys. Chem. C*, 2007, **111**, 4847.
46. K. Cao, J. Lu, J. Cui, Y. Shen, W. Chen, G. Alemu, Z. Wang, H. Yuan, J. Xu, M. Wang and Y. Cheng, *J. Mater. Chem. A*, 2014, **2**, 4945.
47. Y. Cao, Y. Bai, Q. Yu, Y. Cheng, S. Liu, D. Shi, F. Gao and P. Wang, *J. Phys. Chem. C*, 2009, **113**, 6290.
48. Z.-M. Tang, T. Lei, K.-J. Jiang, Y.-L. Song and J. Pei, *Chem. Asian J.*, 2010, **5**, 1911.
49. Y. Wu, X. Zhang, W. Li, Z.-S. Wang, H. Tian and W. Zhu, *Adv. Energy Mater.*, 2012, **2**, 149.
50. M. Zhang, Z. Yao, C. Yan, Y. Cai, Y. Ren, J. Zhang and P. Wang, *ACS Photon.*, 2014, **1**, 710.
51. A. Yella, C.-L. Mai, S. M. Zakeeruddin, S.-N. Chang, C.-H. Hsieh, C.-Y. Yeh and M. Grätzel, *Angew. Chem. Int. Ed.*, 2014, **53**, 2973.
52. E. J. Palomares, L. Cabau, V. K. Challuri, A. Moncho, J. N. Clifford and N. Lopez, *Energy Environ. Sci*, 2015, **8**, 1368.
53. D. P. Hagberg, J.-H. Yum, H. Lee, F. De Angelis, T. Marinado, K. M. Karlsson, R. Humphry-Baker, L. Sun, A. Hagfeldt, M. Grätzel and M. K. Nazeeruddin, *J. Am. Chem. Soc.*, 2008, **130**, 6259.
54. B. C. O'Regan, K. Walley, M. Juozapavicius, A. Anderson, F. Matar, T. Ghaddar, S. M. Zakeeruddin, C. Klein and J. R. Durrant, *J. Am. Chem. Soc.*, 2009, **131**, 3541.
55. Z. Zhang, S. M. Zakeeruddin, B. C. O'Regan, R. Humphry-Baker and M. Grätzel, *J. Phys. Chem. B*, 2005, **109**, 21818.
56. B. C. O'Regan and J. R. Durrant, *Acc. Chem. Res.*, 2009, **42**, 1799.
57. J. N. Clifford, E. Martinez-Ferrero and E. Palomares, *J. Mater. Chem.*, 2012, **22**,

12415.
58. F. Sauvage, S. Chhor, A. Marchioro, J.-E. Moser and M. Grätzel, *J. Am. Chem. Soc.*, 2011, **133**, 13103.
59. B.-S. Chen, K. Chen, Y.-H. Hong, W.-H. Liu, T.-H. Li, C.-H. Lai, P.-T. Chou, Y. Chi and G.-H. Lee, *Chem. Commun.*, 2009, 5844.
60. S.-W. Wang, C.-C. Chou, F.-C. Hu, K.-L. Wu, Y. Chi, J. N. Clifford, E. J. Palomares, S.-H. Liu, P.-T. Chou, T. C. Wei and T. Y. Hsiao, *J. Mater. Chem. A*, 2014, **2**, 17618.

TOC illustration:

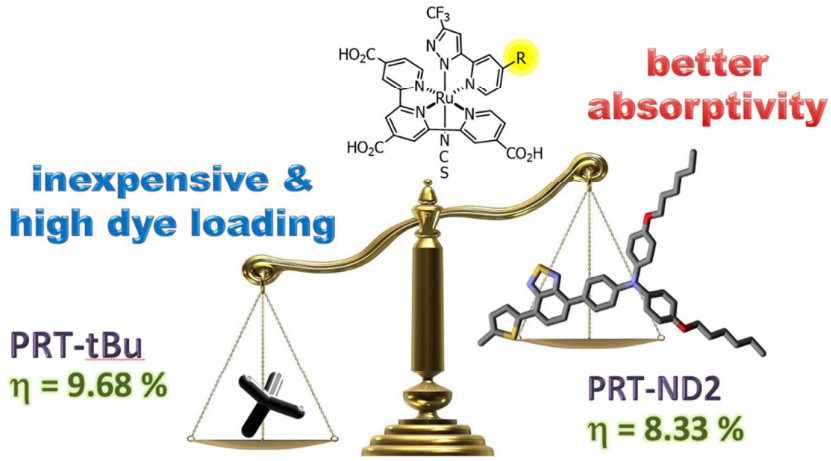

Sensitizer PRT-tBu is the best candidate for fabrication of DSC device after taking into the consideration of relative performances, device stability and scaled-up production capability.